Available online at www.sciencedirect.com
ScienceDirect
Journal of Power Sources 167 (2007) 472–481
JOURNAL OF POWER SOURCES
www.elsevier.com/locate/jpowsour

Perovskite catalysts for the auto-reforming of sulfur containing fuels

Peter Dinka, Alexander S. Mukasyan *

Department of Chemical and Biomolecular Engineering, Center for Molecularly Engineered Materials, University of Notre Dame, Notre Dame, IN 46556, United States

Received 11 January 2007; received in revised form 14 February 2007; accepted 15 February 2007
Available online 2 March 2007

Abstract

The ideal fuel for PEMs and SOFC fuel cells is pure hydrogen, which is not available in nature and thus needs to be produced from other resources. It is a special task to make hydrogen from JP-8 (kerosene-based jet propulsion fuel), which consists of high hydrocarbon and aromatic compounds, as well as contains a significant amount of sulfur (up to 3000 ppm). The auto-thermal reforming (ATR) process is externally energy-intensive and cost-effective method for hydrogen generation. However, it is critical to develop highly efficient, low-cost catalyst. This paper presents a detailed description of a novel combustion approach for synthesis of complex $LaFeO_3$-based catalysts. The activities of these catalysts for ATR of JP-8 fuel were also tested in unique Micro-Scale Bench-Top Reactor System. Several non-noble (Me = K, Na, Li, Cs, Co, Mo) and noble metals additives (Me = Pt, Pd, Ru, Re) were tested as B-site substitution in $La_{0.6}Ce_{0.4}Fe_{0.8-Z}Ni_{0.2}Me_ZO_{3-\delta}$ perovskite to find the compositions that possess stable and effective performance under severe sulfur containing environment. It was shown that small amounts of potassium (2 wt.%) or ruthenium (1 wt.%) doped to above perovskite structure significantly increase catalysts activity and lead to their stable performance during reforming of JP-8 fuel with up to 220 ppm of sulfur.

Keywords: Hydrogen; Auto-thermal reforming; Perovskite; Combustion synthesis

1. Introduction

Fuel cell energy systems have attracted attention due to their high efficiency and zero-emission. Proton exchange membrane and solid oxide fuel cells in the stationary and auxiliary power units are the most promising approaches. The ideal fuel for such cells is *pure hydrogen*, which is not available in nature and thus needs to be produced from other resources. The technical limitations associated with difficulties of hydrogen transportation, storage, and handling suggest the in-sight hydrogen production from liquid organic fuels.

It is a special task to make hydrogen from JP-8, which is kerosene-based jet fuel [1]. It has been estimated that approximately 60 billion gallons of this fuel are used worldwide each year, with 4.5 billion used by the US Air Force, the US Army and NATO. The military has no current plants to add hydrogen to the strategic and tactical operations logistics burden, and therefore the challenge is the on-board reforming of the existing prevalent JP-8 military fuel to produce hydrogen. However, it is very difficult to reform such a fuel, because it involves high hydrocarbon, as well as aromatic compounds. Moreover, it also contains a significant amount of sulfur (up to 3000 ppm). It is well recognized that the fuel with such composition has a vast tendency to a *carbon formation on catalyst*, which leads to catalyst rapid poisoning and reaction termination [2,3].

To remove the sulfur from the fuel by so-called hydrodesulfurization (HDS) process is also not an easy task. The HDS involves several long-term cycles and still significant amount of sulfur 5–100 ppm remains in the fuel [4]. Thus to find an effective catalyst for reforming of high-hydrocarbon fuel containing sulfur is a critical task.

The conversion of hydrocarbon fuels to H_2 can be carried out by several catalytic reactions, including steam reforming (SR) (reaction (1)), catalytic partial oxidation (CPO) (reaction (2)) and auto-thermal reforming (ATR) which *combines* SR and CPO reactions. The SR has high hydrogen yield, but it is an endothermic reaction. The CPO is highly exothermic, but yields less hydrogen. Also, it is well known that a presence of oxygen decreases coke deposition on catalyst [5]. Thus, ATR process is less externally energy-intensive and cost-effective than other conventional processes [6], and thus can be considered as a

* Corresponding author. Tel.: +1 574 631 9825; fax: +1 574 631 8366.

0378-7753/$ – see front matter © 2007 Elsevier B.V. All rights reserved.
doi:10.1016/j.jpowsour.2007.02.058

promising approach for hydrogen generation. Note, that simultaneously with reactions (1) and (2) two additional reactions take place during ATR; i.e. water-shift reaction (3), which increases hydrogen yield and undesired hydrogen consuming methanation (4):

$$C_nH_m + nH_2O \rightarrow nCO + (n + 0.5m)H_2 \quad (1)$$

$$C_nH_m + 0.5nO_2 \rightarrow nCO + 0.5mH_2 \quad (2)$$

$$CO + H_2O \rightarrow H_2 + CO_2 \quad (3)$$

$$CO + 3H_2 \rightarrow CH_4 + H_2O \quad (4)$$

To make fuel cells commercialization, it is critical to develop highly efficient, low-cost catalyst for ATR. Indeed, the conventional Ni-based catalysts for SR are rapidly deactivated in the case of sulfur-containing fuels. Hence, bimetallic catalysts involving expensive noble metals, such as Pt, Rh, and Ru were recently developed [7–9]. However, their high cost and limited yield inhibit their extensive usage. The same obstacles are related to the non-pyrophoric precious metal catalysts such as Pt/CeO_2-ZrO_2 [10] or $Pt/ZrO_2/Al_2O_3$ [11] compositions.

Complex mixed metal oxides with *perovskite* structure attract significant interest in many areas of solid-state chemistry including catalysis [12–14]. Specific application of perovskites in ATR of heavy hydrocarbons was studied in Argon National Laboratories [8,15,16]. The general formula of perovskites is ABO_3, where A is a metal with lager ionic radii, typically from rare-earth group and B is a metal with smaller radii, usually from transition metals group. Partial substitution of A, B or both sites allows one to synthesize a wide variety of compositions with different properties.

In previous work [17] we have investigated the $LaFeO_3$ perovskites substituted by cerium (A-site) and nickel (B-site) as potential low cost coking-resistant catalysts for ATR of a *sulfur-free* JP-8 fuel surrogate. It was shown that such catalysts exhibit excellent stability during autothermal reforming at 775 °C, with near-equilibrium hydrogen yield even at relatively high gas hourly space velocity value (GHSV = 130,000 h^{-1}). However, further experiments show that presence of small amounts of sulfur (>10 ppm) in fuel dramatically decrease its activity. The purpose of this paper is to provide a description of the preparation method and characterization tests for modified $LaFeO_3$-based catalysts that show high activity and stable performance during reforming of JP-8 fuels with up to 220 ppm of sulfur.

2. Experimental

2.1. Catalyst preparation

Different techniques are used for perovskite preparations, including sol–gel [18], solid-state [19] and mechano-synthesis [20] methods, as well as *combustion synthesis* [21]. The latter is an attractive approach for production of advanced solid-state materials. The specific feature of this technique is that after its local initiation, a self-sustained reaction propagates throughout the heterogeneous powder reactive mixture, leaving behind the desired products. Modification of this technique, so-called *solution combustion* (SC) synthesis, takes place in a aqueous solution of the oxidizers (e.g. metals nitrites) and fuels (e.g. glycine, citric acid and urea) [21,22]. In conventional scheme, at certain temperature (100–200 °C) the reaction self-ignites through the entire reactive media (so-called volume combustion synthesis (VCS) mode) leading to the formation of fine solid products with tailored composition. Under equilibrium conditions, in general such combustion reactions can be represented as follows:

$$Me^{\nu}(NO_3)_{\nu} + \left(\frac{5}{9}\nu\phi\right) CH_2NH_2CO_2H + \nu\frac{5}{4}(\phi - 1)O_2 \Rightarrow MeO^{(s)}_{\nu/2} + \left(\frac{10}{9}\nu\phi\right) CO_2^{(g)} + \frac{25}{18}\phi H_2O^{(g)} + \nu\frac{(5/9\phi + 1)}{2} N_2^{(g)}$$

where Me^{ν} is a metal with valence ν and ϕ is a fuel to oxidizer ratio, $\phi = 1$ means that the initial mixture does not require atmospheric oxygen for complete oxidation of fuel, while $\phi > 1$ (<1) implies fuel-rich (lean) conditions.

Recently we developed novel modifications of the solution combustion synthesis [23]. These methods include:

1. *Self-propagating sol–gel combustion* (SSGC) [24]: the desired amount of metals nitrates + fuel solution is dried at room temperature to make a sol–gel like heterogeneous media, which was than *locally ignited* with the help of a heated tungsten wire. As a result a self-sustained reaction wave steadily propagates along the media forming nano-powder of desired composition. This *steady-state* propagating *mode* allows more *precise control* of the material composition and structure as compared to conventional VCS scheme, which proceeds by thermal *explosion*.
2. *Impregnated support combustion* (ISC) method involves impregnation of reaction solution inside the porous structure of the inert solid support, followed by reaction initiation similar to those in SSGC mode. ISC permits synthesize of supported catalyst with extremely high surface areas (up to 200 $m^2\ g^{-1}$) [25].
3. *Impregnated active layers combustion* (IALC) method [23,26]. In this case, the reaction solution is impregnated, for example, into *thin*, pure cellulose paper and dried at room temperature. Further, such paper is locally ignited at room temperature and steady-state combustion front propagates along the reactive media. The maximum reaction temperature can be as high as 1000 °C, but reaction time owing to the rapid quenching of thin reacted layer, is less than 0.1 s. The latter leads to high surface area of the synthesized catalyst. Note, that amount of residual carbon in as-prepared materials by IALC approach does not exceed 0.1 wt.%. Comparison of the catalysts prepared by different approaches mentioned above allowed us to conclude that IALC-catalysts possess the highest activity and stability for ATR [23].

Based on IACL approach the apparatus, which allows continuous production of catalyst was designed and built [26]. The scheme of the set-up is presented in Fig. 1. Briefly, a paper from

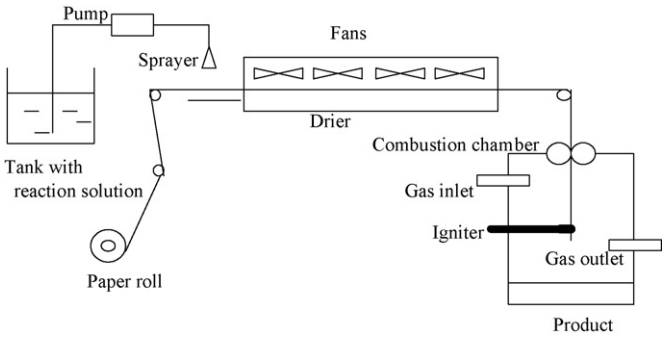

Fig. 1. Scheme of set-up for impregnated active layers combustion synthesis.

a role (1) supported by transporter (2) elevated to the area (3) where spray-nozzles are located. The reactive aqueous solution from a tank (4) is delivered by peristaltic pump (5) to the nozzles, which uniformly sprayed solution on the paper. The paper with impregnated solution is further transported to the dryer (6), which is equipped with temperature-controlled furnace and two fans. Dried paper enters the combustion chamber (7), where it is ignited by electrically heated wire. It is important that impregnation and drying processes can be adjusted is such a way that the speed of paper movement is exactly equal to the velocity of the reaction front that propagates along the reactive media. As a result, position of the reaction is spatially stabilized in the middle part of the combustion chamber. The synthesized material is collected in the lower part of the chamber in the attached tray (8).

Using this approach a variety of $LaFeO_3$-based perovskite were synthesized (see Fig. 2). The different metal nitrates $Me(NO_3)_x$ (where Me = La, Ce, Fe, Ni, etc.; Alfa Aesar) and glycine $C_2H_5NO_2$ (98%, Alfa Aesar) were used as the precursors. The specific surface area was measured using BET (Quantachrome, Autosorb-1), while the crystallinity and phase composition were determined by XRD analysis (X1 Advanced Diffraction System, Scintag Inc.). The composition of catalysts was analyzed by means of ICP analysis (Perkin-Elmer/Sciex Elan DRCe ICP-MS). XPS analysis was also conducted using a Kratos Analytical ESCA system with monochromatic Mg Kα X-rays of 1253.6 eV. Finally, the carbon and sulfur content was evaluated by elemental combustion analysis (Costech Analytical Technologies Inc.).

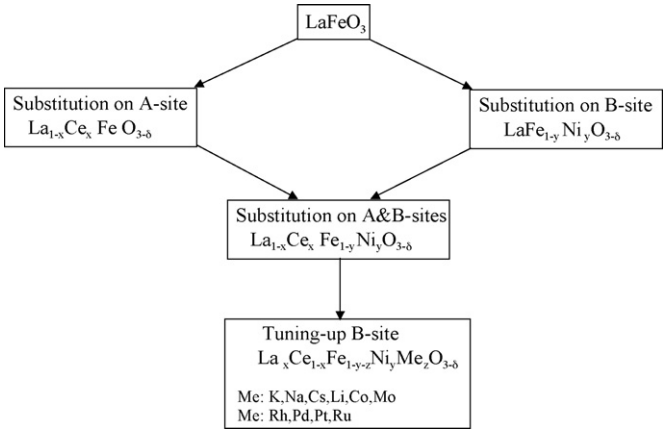

Fig. 2. Chart of synthesized perovskites.

2.2. Fuel preparation

Two different fuels were used, i.e. JP-8 and its surrogate. The composition of surrogate was based on the work of Montgomery et al. [27]. This representative blend, in molar percent contains 34.7% *n*-dodecane, 32.6% *n*-decane, 16.7% methylcyclohexane and 16.0% terc-butyl benzene. To control amount of sulfur in fuel the desired quantity of 1,4-thioxane (C_4H_8OS) was added to the surrogate.

A desulfurization module (see Fig. 3) was built and used for purifying the JP-8 fuel, which initially contains ∼1000 ppm of sulfur. The unit consists of series of two tubular reactors. Upper reactor was charged with cobalt-based desulfurization catalyst (Engelhard, USA). Prior to entering the reactor, the fuel was dosed by isocratic digital pump (Lab Alliance, Series III, USA) and mixed with hydrogen, which was also quantified by mass flow controller (Brook Instrument, USA). The reactor is thermostated at temperature 300 °C by electrical furnace. The outgoing flow is air-cooled and enters the lower reactor filled with adsorption material to capture H_2S release. The pressure (∼2 MPa) is controlled by valve at the outlet of the reactor. The desulfurized fuel was collected in tank and used for the experiments. The JP-8 was cleaned up multiple times to produce fuels with different amount of sulfur. The decrease of sulfur content as a function of number of cleaning cycles is shown in Fig. 4.

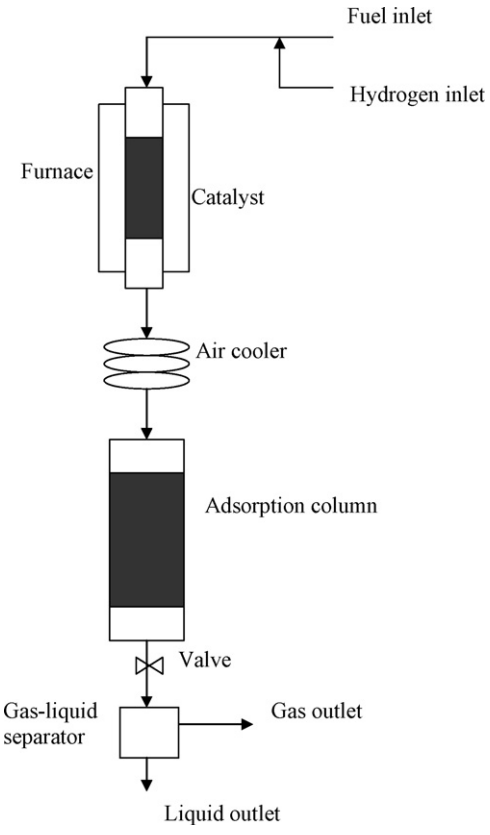

Fig. 3. Scheme of desulfurization unit.

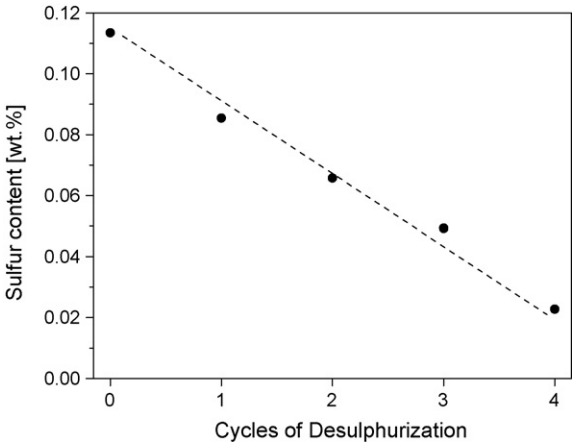

Fig. 4. Sulfur content in fuel vs. cycles of desulfurization.

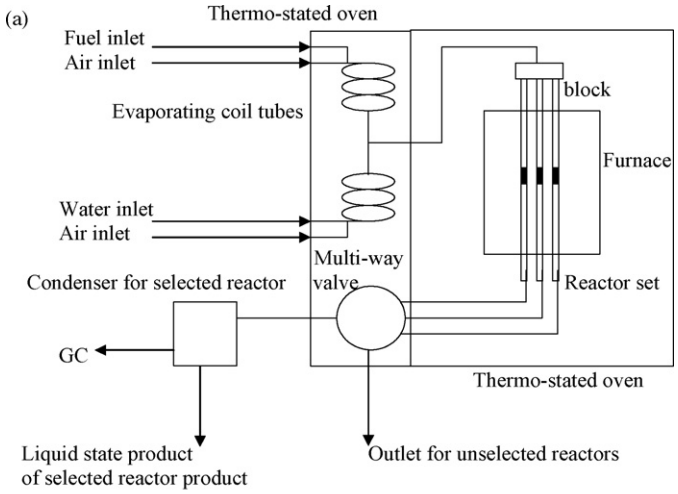

Fig. 5. Scheme (a) and picture (b) of Micro-Scale Bench-Top Reactor System.

2.3. Catalyst tests

High-throughput catalysis, which only in the last years became feasible as a result of advances in micro-fabrication, computing and instrumentation, allows one by rapid exploration of the large database to significantly accelerate the process of catalysts discovery and optimization [28]. In this work in combination with effective material synthesis approach, described above, we also used Micro-Scale Bench-Top Reactor System (BTRS), which is a high-throughput device for testing the catalyst activity. This apparatus was designed and built in collaboration with Autoclave Engineers Inc. (Erie, OH, USA). The scheme and picture of the BTRS are shown in Fig. 5. Automatic multi-step acquisition system, built based on the integral micro-processor, provides independent programming for eight tubular reactors, as well as GC analysis of gas phase products. The following ranges of conditions can be used for a long-term unattended operation: gas pressure 0.1–2 MPa and temperature up to 1000 °C.

Prior to carrying out the reaction, the catalysts were activated at temperature of 800 °C (heating at 10 °C min^{-1}) for 2 h under a flow of reduction gas (5 mol.% H_2 in N_2). After reduction the hydrogen flow was terminated and reactants (fuel, water and air) were introduced to the system. Water and fuel were separately mixed in desired amounts with air and continuously evaporated in coiled tubes located in oven thermostated at ~250 °C. The evaporated fuel and steam were than mixed and entered a distribution block, where the reactant flow was evenly spread into eight tubular parallel reactors (7 mm i.d.). Distribution block involves eight orifices, which are located on the entrances to each reactor. Having very small inner diameter (50 μm) these orifices insure high pressure-drop and thus even distribution of fuel mixture among all reactors (Fig. 5a and b). The reactors are also uniformly heated by programmed electrical furnace, providing the similar temperature-time schedule in all reaction volumes. In addition the whole reactor assembly is isothermally thermostated at 300 °C to prevent reactants condensation.

A heated multi-port valve-set is used to periodically select one of the eight reactors' out-streams and to transfer the reaction product to gas/liquid separator. The latter is attached to on-line high-speed Micro GC (Agilent Micro GC 3000A) that allows continuous gas products analysis. The two channels Micro GC is equipped with Molecular Sieve and Plot Q columns with argon and helium as a gas carrier, respectively. The thermal conductivity detectors are used in both channels. Because liquid hydrocarbon residuals could not be analyzed in such assay, nitrogen was used as an inert standard for determination of the total carbon concentration in gas phase products.

Based on the thermodynamic analysis and experiments [17], the following operational conditions were used: $H_2O/C = 3$, $O_2/C = 0.35$, at a temperature 800 °C and relatively high GHSV = 130,000 h^{-1}. This high-throughput approach is convenient for rapid screening of activity for a large number of different catalysts. However, thus depicted, best catalysts were additionally tested under similar conditions in a single fixed-bed reactor, which was described elsewhere [17].

Catalytic activity was evaluated in terms of fuel conversion and hydrogen content in gas phase product by an internal standard (nitrogen in air) analyzing method. Indeed, the inlet and outlet nitrogen flow-rates remain constant during the test, while the outlet overall flow-rate changes as a result of chemical reactions. The conversion was calculated as ratio of the total amount

of carbon in gaseous products and carbon in the fuel:

$$\text{Converison}\,(\%) = \frac{F(\text{CO}) + F(\text{CO}_2) + F(\text{CH}_4)}{F(\text{C}_{\text{Fuel}})} \times 100\%,$$

where $F(\text{CO})$, $F(\text{CO}_2)$, $F(\text{CH}_4)$ represents flow-rates of CO, CO_2, CH_4 in gas product, respectively, and $F(\text{C}_{\text{Fuel}})$ is a flow-rate of carbon in a fuel. In turn, the absolute values of $F(\text{CO})$, $F(\text{CO}_2)$ and $F(\text{CH}_4)$ were calculated as follows:

$$F(i) = \frac{F(\text{N}_2)\, X(i)}{X(\text{N}_2)},$$

where $X(i)$ and $X(\text{N}_2)$ are the mole fractions of compound i (CO, CO_2 and CH_4) and N_2, respectively, in gas product.

However, the hydrogen content in gas phase product can be also calculated based on measured amount of CO, CO_2 and CH_4 assuming that H_2 formation occurs through reactions (1)–(4). The expression used to calculate the amount of hydrogen is derived in Appendix A. The comparison of experimentally measured and calculated values shows their very good agreements (Table A1). The latter indicates that suggested overall reaction scheme (1)–(4) describes well the considered ATR process.

3. Results and discussion

The XRD patterns for some of synthesized perovskites are shown in Fig. 6. It can be seen that in all cases the well-crystallized perovskite structures were formed directly in the combustion wave. However, in the catalysts containing cerium, in addition to the perovskite phase, small amount of Ce_7O_{12} was detected. Example of ICP analysis and calculated values for $La_{0.6}Ce_{0.4}Fe_{0.8}Ni_{0.2}O_3$ catalyst are shown in Table 1. The measured and theoretically expected values are in good agreement. These data indicate that the IACL method is efficient approach for direct synthesis of the complex oxides with desired composition.

As it was mentioned in Section 1 the substituted La-Fe-O-based perovskites were shown to be excellent catalysts for ATR of JP-8 surrogate with near-equilibrium hydrogen yield [17]. However, the experiments indicate (see Fig. 7) that presence of small amounts of sulfur (e.g. 50 ppm) in fuel significantly decreases its activity (i.e. conversion drops below 60%). Thus, several non-noble (Me = K, Na, Li, Cs, Co, Mo) and noble metals additives (Me = Pt, Pd, Ru, Re) were tested as B-site substitution to find the compositions that perform well under severe sulfur containing environment.

Table 1
Data of ICP analysis and theoretically calculated values for of $La_{0.6}Ce_{0.4}Fe_{0.8}Ni_{0.2}O_3$ catalyst

Element	Metal content [wt.%]	
	ICP measurement	Calculated
La	34.4	34.4
Ce	23.1	22.6
Fe	18.4	15.1
Ni	4.8	4.5

3.1. Non-noble metal additives

The BET surface areas (SA) of the as-synthesized materials are presented in Table 2. Only Li-containing material has low SA $\sim 1\ m^2\ g^{-1}$, while other perovskites are characterized with relatively high SA (10–20 $m^2\ g^{-1}$) for these types of compositions.

Fuel conversion and hydrogen content in gas phase products for JP-8 surrogate containing 50 ppm of sulfur for catalysts ($La_{0.6}Ce_{0.4}Fe_{0.8-Z}Ni_{0.2}Me_ZO_{3-\delta}$) with different metal (Me) are also presented in Fig. 7. It was shown that except for molybdenum (Mo), all tested additives have favorable effect on catalytic activity of the used perovskites. However, among them potassium (K) and cobalt (Co) show the highest efficiency, achieving conversion and hydrogen content ~75 and ~30%, respectively. It can be seen from Table 2 that SA of these catalysts dropped from 20 to ~4 $m^2\ g^{-1}$ during ATR process, because high temperature in presence of steam promotes material sintering [29]. However, this drop rapidly occurs during the first hours (1–2 h) of the process, followed by stabilization of materials properties, i.e. SA remains essentially constant after 24 h high-temperature treatment.

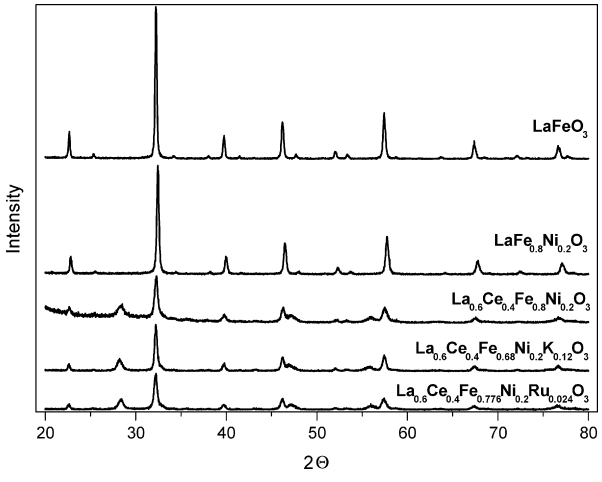

Fig. 6. XRD patterns for different synthesized perovskites.

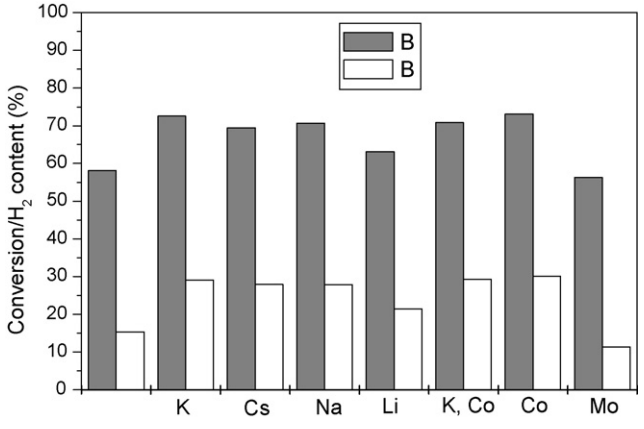

Fig. 7. Conversion and hydrogen content vs. metal additive (JP-8 surrogate containing 50 ppm of sulfur).

Table 2
Some properties for various $La_{0.6}Ce_{0.4}Fe_{0.8-Z}Ni_{0.2}Me_ZO_{3-\delta}$ (2 wt.% of Me) catalysts

Additive	Surface area as synthesized [$m^2\ g^{-1}$]	Surface area after ATR [$m^2\ g^{-1}$]	C content as synthesized [wt.%]	C content after ATR [wt.%]
–	20.9	5.1	0.15	0.04
K	15.2	4.1	0.17	0
Cs	19.3	4.9	0.15	0
Na	8.1	2.2	0.14	0
Li	1.7	0.8	0.07	0
K + Co	14.9	4.2	0.19	0
Co	22.5	5.3	0.10	0
Mo	22.3	4.5	0.08	4.1

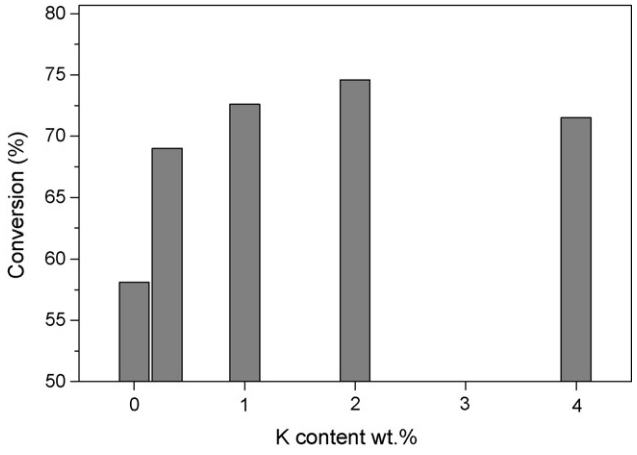

Fig. 8. Conversion vs. amount of K additive to $La_{0.6}Ce_{0.4}Fe_{0.8-Z}Ni_{0.2}M_ZO_{3-\delta}$ catalyst (JP-8 surrogate containing 50 ppm of sulfur).

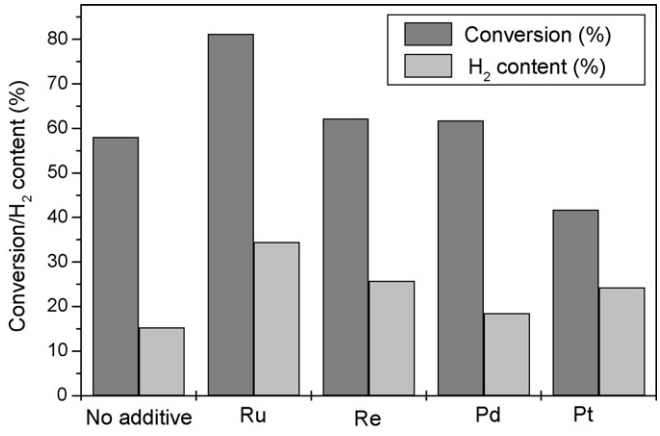

Fig. 9. Conversion and hydrogen content vs. noble metal additive (JP-8 surrogate containing 50 ppm of sulfur).

It is also important that carbon content in all catalysts (except of Mo-containing) after the reaction is essentially zero, thus being lower then for as-synthesized materials (Table 2). This result demonstrates the high efficiency of carbon removal from catalyst surface owing to presence of oxygen vacancies in perovskite phases [30]. Based on the above data $La_{0.6}Ce_{0.4}Fe_{0.8-Z}Ni_{0.2}K_ZO_{3-\delta}$ catalyst was selected for further tests, since it also shows more stable activity, as compared to Co-containing compositions, during the long-term runs.

Effect of potassium amount (x) in $La_{0.6}Ce_{0.4}Fe_{0.8-Z}Ni_{0.2}Me_ZO_{3-\delta}$ composition on conversion of JP-8 surrogate with 50 ppm of sulfur is shown in Fig. 8. It can be seen that addition of small amount of potassium (0.33 wt.%) significantly increases catalyst activity (from 58 to 69%). Another enhancement of activity (up to 75%) is observed by increasing K content up to 2 wt.% (see Fig. 8). Also note that catalysts without or small amount of potassium show the presence of carbon after the ATR run, while for compositions containing ≥1 wt.% of K no carbon was detected (Table 3). These results suggest that 2 wt.% of K is an optimum amount of the metal additive to the perovskite structure.

3.2. Noble metal additives

Conversion and hydrogen content in gas phase product for ATR of JP-8 surrogate containing 50 ppm of sulfur using $La_{0.6}Ce_{0.4}Fe_{0.8-Z}Ni_{0.2}Me_ZO_{3-\delta}$ catalyst (where Me is a noble metal in amount of 2 wt.%) are summarized in Fig. 9. Surprisingly, significant decrease of conversion was observed (42%) when platinum (Pt) was used as an additive. In addition high amount (7.2 wt.%) of carbon was detected on this catalyst after ATR. Rhenium and palladium lead only to minor enhancement in catalyst activity, while again considerable coking (11.9 and

Table 3
Some properties for $La_{0.6}Ce_{0.4}Fe_{0.8-Z}Ni_{0.2}K_ZO_{3-\delta}$ catalysts

K content [wt.%]	SA calculated 800 °C, 2h [$m^2\ g^{-1}$]	SA after reaction [$m^2\ g^{-1}$]	C content calculated 800 °C, 2h [wt.%]	C content after reaction [wt.%]
–	20.9	5.1	0.15	0.04
0.3	14.2	4.0	0.13	0.03
1	19.0	3.6	0.13	0
2	15.2	4.1	0.17	0
4	9.6	3.6	0.18	0

Table 4
Some $La_{0.6}Ce_{0.4}Fe_{0.8-Z}Ni_{0.2}M_ZO_{3-Y}$ properties with various noble metal additives in amount of 2 wt.% before and after catalytic test

Additive	Surface area [$m^2\ g^{-1}$]	Surface area after reaction [$m^2\ g^{-1}$]	C content [wt.%]	C content after reaction [wt.%]
Ru	17.6	4.4	0.01	0
Re	20.7	4.5	0.15	11.94
Pd	35.6	8.5	0.05	6.76
Pt	23.4	11.2	0.26	7.2

6.8 wt.%, respectively) was observed (Table 4). On the other hand, significant improvements in conversion (81%) and hydrogen yield (35%) were obtained with ruthenium as an additive. Moreover, no carbon was detected on this catalyst after the ATR reaction.

Influence of ruthenium content in complex $La_{0.6}Ce_{0.4}Fe_{0.8-Z}Ni_{0.2}Ru_ZO_{3-\delta}$ perovskite on conversion of JP-8 surrogate containing 50 ppm of sulfur is shown in Fig. 10. Even small amount of ruthenium (0.5 wt.%) increases conversion from 58 to 75%, approaching the saturation of ~81% for ≥1 wt.% Ru. Taking into account the cost consideration the composition with 1 wt.% of Ru was selected as an optimum for further analysis.

3.3. Optimization of Ni content

It is known, that the active part of catalysts for steam reforming or ATR is nickel [31]. However, nickel has also high tendency for coking [32,33]. To avoid latter effect the complex perovskite-nickel catalyst was developed. Indeed, it was shown that during reduction stage Ni phase appeared on the perovskite surface. Fig. 11 compares the phase compositions of the initial (a) and reduced (b) $La_{0.6}Ce_{0.4}Fe_{0.68}Ni_{0.2}K_{0.12}O_{3-\delta}$ perovskite. The presence of Ni peaks after reduction confirms that complex metal/oxide catalyst has been formed. Ideally a good contact between nickel sites and oxygen conductive surface is required for efficient use of active oxygen for carbon removal [30]. This effect is more pronounced for the small size of formed Ni particles, which in turn depends on the amount of Ni in the initial perovskite structure: more Ni leads to larger size of metal sites. Thus, on one hand, higher nickel content in perovskite should

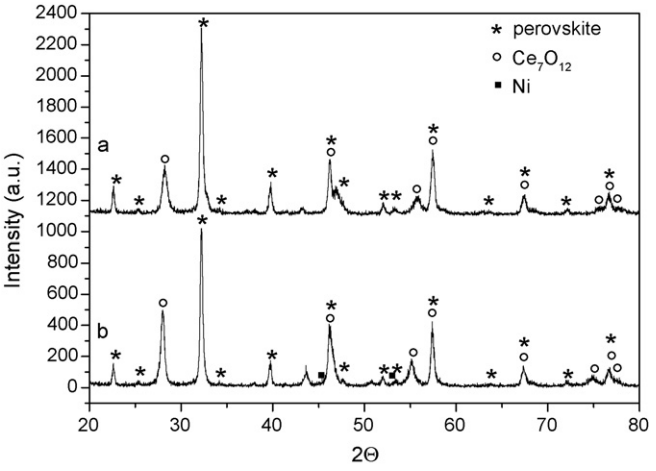

Fig. 11. XRD patterns of $La_{0.6}Ce_{0.4}Fe_{0.68}Ni_{0.2}K_{0.12}O_{3-\delta}$ perovskite after: (a) calcination (800 °C, 2 h) and (b) reduction (800 °C, 2 h, rump 10 °C h^{-1}).

lead to higher intrinsic catalyst activity. On the other hand, it may result in much faster coking of catalyst.

To optimize perovskite composition for considered ATR process the conversion, hydrogen content and carbon amount after test in $La_{0.6}Ce_{0.4}Fe_{0.68-Y}Ni_YK_{0.12}O_{3-\delta}$ catalyst with various y (from 0 to 0.6) was investigated (Fig. 12). It can be seen that with increasing amount of Ni, activity of catalysts indeed increases: from 65% conversion for catalyst without nickel ($y = 0$) up to 75% for $x = 0.6$. However, the analysis on carbon content in cat-

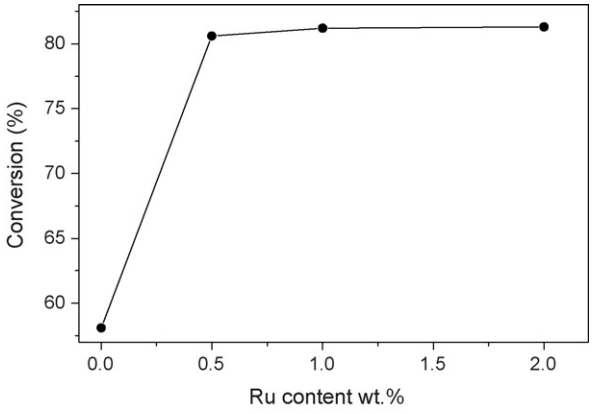

Fig. 10. Conversion vs. amount of Ru additive to $La_{0.6}Ce_{0.4}Fe_{0.8-Z}Ni_{0.2}Ru_ZO_{3-\delta}$ catalyst (JP-8 surrogate containing 50 ppm of sulfur).

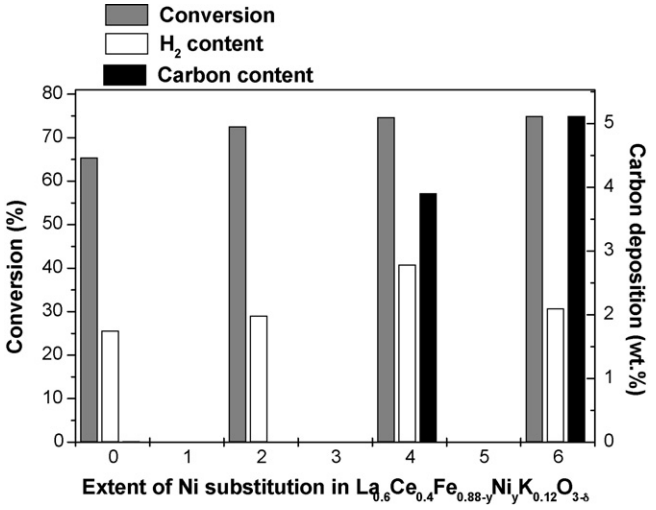

Fig. 12. Conversion and carbon deposition vs. amount of Ni in $La_{0.6}Ce_{0.4}Fe_{0.68-Y}Ni_YK_{0.12}O_{3-\delta}$ catalyst (JP-8 surrogate containing 50 ppm of sulfur).

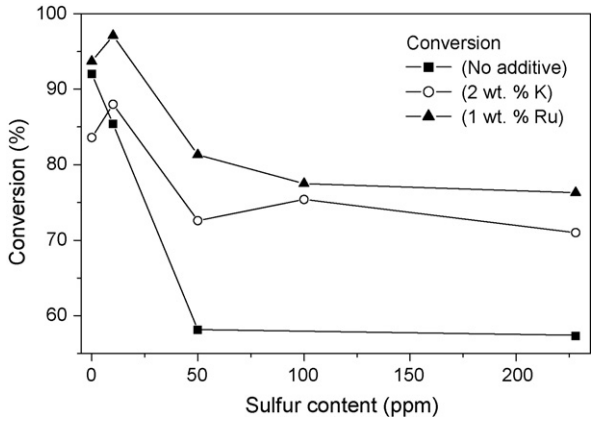

Fig. 13. Conversion vs. sulfur content in fuel for $La_{0.6}Ce_{0.4}Fe_{0.8}Ni_{0.2}O_3$ catalysts with and without (2 wt.% of K and 1 wt.% of Ru) doping.

alysts after ATR indicates that higher nickel amount leads to much more rapid coking. Note, that essentially no carbon was detected on catalysts with $0 \leq y \leq 0.2$. Thus, composition $y = 0.2$ was selected as an optimum.

3.4. Influence of sulfur content in fuel on catalyst activity

Dependences of conversion versus amount of sulfur in fuel for $La_{0.6}Ce_{0.4}Fe_{0.8-Z}Ni_{0.2}$ $Me_ZO_{3-\delta}$ catalysts without metal (Me) additive ($x = 0$) and with 2 wt.% of K and 1 wt.% of Ru are shown in Fig. 13. It can be seen that the efficiency of all tested catalysts for fuel with ≤10 ppm of sulfur is relatively high 85–95%. Interestingly that the small sulfur amount even increases activity of catalysts containing K and Ru. Note that similar effect was observed previously [34]. As noted above, the activity of catalyst without additives with fuels containing more than 10 ppm of sulfur significantly decreases. At the same time the catalysts with K and Ru show much higher conversions for these fuels, e.g. 75 and 82%, respectively, for 50 ppm of sulfur. It is important that for fuels with higher sulfur content (up to 228 ppm) only small drops in catalyst activities were observed. Note that last points in Fig. 13 (228 ppm of sulfur) belong to real desulfurized JP-8.

It is critical to understand the influence of small amount of K and Ru additives on the complex catalyst activity. For this purpose XPS analysis were done to obtain the electronic state of K and Ru. Unfortunately owing to the difficulties of data treatment in complex catalysts structure reliable results were not obtained. Thus, at this stage it can only be presumed that the unique behavior of Ru doped perovskite occurs due to alloying of Ni with Ru to form the highly active bimetallic Ni–Ru sites. Research addressing this issue by using EXAFS fine structural measurements and investigating long-term (1000 h) catalysts treatment are under progress.

4. Conclusion remarks

An efficient material screening strategy, which includes novel combustion-based method for catalyst synthesis and high-through approach for their activity characterization, was developed and used for searching a low cost catalyst for ATR of JP-8 fuel to produce hydrogen. It was proved that complex perovskite (ABO_3)-based catalysts can be very effective for ATR of heavy hydrocarbons. Specifically, it was demonstrated that for $LaFeO_3$—basic composition, a partial substitution of La by Ce on A-side enhances catalyst ability for carbon removal, while corresponding B(Fe)-site substitution by Ni leads to increasing of its catalytic activity. However, the presence of sulfur in fuel gives special demand on material, since S easily deactivates the catalysts. As a result of wide search for different compositions, it was concluded that small amount of metal additives can increase stability of perovskite-based catalysts in sulfur containing environment. For example, it was found that 2 wt.% of potassium or 1 wt.% of ruthenium substituted on B-side of the $La_{0.6}Ce_{0.4}Fe_{0.68-Y}Ni_yO_{3-\delta}$ significantly increases its durability during ATR of JP-8 fuel. Thus, the presented work covers an important aspect of the hydrogen economy and we believe that obtained results hold a key to low cost-effective catalysts for production of hydrogen from sulfur containing fuels.

Acknowledgement

This work was supported by the U.S. Army CECOM RDEC through Agreement DAAB07-03-3-K414. Such support does not constitute endorsement by the U.S. Army of the views expressed in this publication.

Appendix A

As mentioned above four reactions are assumed to take place during considered ATR process, i.e. steam reforming of fuel (reaction (A.1)), partial oxidation of fuel (reaction (A.2)), water-shift reaction (A.3) and methanation (A.4), which can be presented in the following forms:

$$\chi_1 C_a H_b + a\chi_1 H_2O \rightarrow a\chi_1 CO + \chi_1 \left(\frac{b}{2} + a\right) H_2 \quad (A.1)$$

$$\chi_2 C_a H_b + \frac{a\chi_2}{2} O_2 \rightarrow a\chi_2 CO + \frac{b\chi_2}{2} H_2 \quad (A.2)$$

$$zCO + zH_2O \rightarrow zCO_2 + zH_2 \quad (A.3)$$

$$yCO + 3yH_2 \rightarrow yCH_4 + yH_2O \quad (A.4)$$

where χ_1 and χ_2 are the extents of (A.1) and (A.2) reactions, respectively.

In this case the overall reaction balance can be presented as follows:

$$\chi_1 + \chi_2 + (1 - \eta)F = F \quad (A.5)$$

where F is a molar amount of fuel and η is the conversion, defined in Section 2.3.

Assume that amounts of formed methane and carbon dioxide are:

$$CH_4 \equiv y \quad (A.6)$$

$$CO_2 \equiv z \quad (A.7)$$

Table A1
Calculated and experimental data on the products' composition

Catalyst	S content in fuel (ppm)	Product composition (%)				H_2 (%)	
		N_2	CH_4	CO	CO_2	Experimental	Calculated
$La_{0.6}Ce_{0.4}Fe_{0.776}Ni_{0.2}Ru_{0.024}O_3$	10	36.1	2.6	12.2	11.5	37.9	37.4
$La_{0.6}Ce_{0.4}Fe_{0.776}Ni_{0.2}Ru_{0.024}O_3$	100	42.6	3.6	6.2	15.4	32.2	32.5
$La_{0.6}Ce_{0.4}Fe_{0.68}Ni_{0.2}K_{0.12}O_3$	10	38.6	3.1	8.8	14.0	35.7	36.1
$La_{0.6}Ce_{0.4}Fe_{0.68}Ni_{0.2}K_{0.12}O_3$	100	43.9	3.8	5.7	15.7	30.9	31.7

In this case an amount of carbon monoxide which is formed in reactions (A.1) and (A.2) and is consumed in reactions (A.3) and (A.4) can be calculated as:

$$\mathrm{CO} \equiv a(\chi_1 + \chi_2) - y - z \tag{A.8}$$

Also amount of hydrogen which is formed in reactions (A.1), (A.2) and (A.3) and is consumed in reaction (A.4) can be expressed as follows:

$$\mathrm{H_2} \equiv \chi_1 \left(\frac{b}{2} + a\right) \frac{b\chi_2}{2} - 3y + z \tag{A.9}$$

where a and b are the carbon and hydrogen indexes, respectively.

Using Eqs. (A.8) and (A.9) extents of reactions χ_1 and χ_2 can be defined as:

$$\frac{\mathrm{CO} + y + z}{a} = \chi_1 + \chi_2 \tag{A.10}$$

$$\frac{\mathrm{H_2} + 3y - z}{b/2} = \left(1 + \frac{2a}{b}\right) \chi_1 + \chi_2 \tag{A.11}$$

By subtracting Eq. (A.10) from Eq. (A.11) one can get:

$$-\frac{\mathrm{CO} + y + z}{a} + \frac{\mathrm{H_2} + 3y - z}{b/2} = \chi_1 \left(\frac{2a}{b}\right) \tag{A.12}$$

Thus, χ_1 can be expressed as:

$$\chi_1 = \frac{\mathrm{H_2} + 3y - z}{a} - \frac{\mathrm{CO} + y + z}{a^2} \frac{b}{2} \tag{A.13}$$

and χ_2 can be expressed as:

$$\chi_2 = \frac{\mathrm{CO} + y + z}{a} + \frac{\mathrm{CO} + y + z}{a} \frac{b}{2a} - \frac{\mathrm{H_2} + 3y - z}{a}$$
$$= \frac{\mathrm{CO} + y + z}{a} \left(1 + \frac{b}{2a}\right) - \frac{\mathrm{H_2} + 3y - z}{a} \tag{A.14}$$

Note that amount of oxygen from reaction (A.2) corresponds to:

$$\mathrm{O_2} = \frac{a\chi_2}{2} \tag{A.15}$$

Defining χ_2 from Eq. (A.15) and substituting it to Eq. (A.14) one can obtain:

$$\frac{2\mathrm{O_2}}{a} = \frac{\mathrm{CO} + y + z}{a} + \frac{(\mathrm{CO} + y + z)(1 + b/2a)}{a} - \frac{\mathrm{H_2} + 3y - z}{a} \tag{A.16}$$

Finally, amount of hydrogen in the product can be calculated from Eq. (A.16) as follows:

$$\mathrm{H_2} = \mathrm{CO}\left(1 + \frac{b}{2a}\right) + \mathrm{CH_4}\left(\frac{b}{2a} - 2\right) + \mathrm{CO_2}\left(2 + \frac{b}{2a}\right) - 2\mathrm{O_2} \tag{A.17}$$

Thus, measuring amounts on CO, CH_4 and CO_2 and knowing amount of oxygen in the fuel mixture it is possible to calculate amount of hydrogen in the final product. However, this value was also measured directly during the reaction. Thus it is interesting to compare experimentally measured values and those calculated under above assumptions. Such comparisons for different experimental conditions are presented in Table A1. As mentioned above, very good agreements between experimental and calculated data are observed.

References

[1] L. Maurice, H. Lander, T. Edwards, W.E. Harrison III, Fuel 80 (2001) 747.
[2] J.R. Rostrup-Nielsen, J. Catal. 31 (1973) 173.
[3] G.J.K. Acres, J. Power Sources 100 (2001) 60.
[4] X. Huang, D.L. King, Ind. Eng. Chem. Res. 45 (2006) 7050.
[5] P.K. Cheekatamarla, A.M. Lane, J. Power Sources 152 (2005) 256.
[6] S. Ahmed, M. Krumpelt, Int. J. Hydrogen Energy 26 (2001) 291.
[7] A. Qi, S. Wang, G. Fu, D. Wu, Appl. Catal. A: Gen. 293 (2005) 71.
[8] K.W. Kramarz, W. Kurt, I.D. Bloom, R. Kumar, S. Ahmed, R. Wilkenhoener, M. Krumpelt, U.S. Patent 5,929,286 (2001).
[9] T. Suzuki, H. Iwanami, T. Yoshinari, Int. J. Hydrogen Energy 25 (2000) 119.
[10] L. Villegas, N. Guilhaume, H. Provendier, C. Daniel, F. Masset, C. Mirodatos, Appl. Catal. A: Gen. 281 (2005) 75.
[11] M.M.V.M. Souza, M. Schmal, Appl. Catal. A: Gen. 281 (2005) 19.
[12] E. Tomoko, N. Yoshihiko, M. Wu, F. Taishi, Patent Appl. Publ. Number US2006210864 (2006).
[13] PR. Javier, V. Bent Erlend, J. Stein, Patent Appl. Publ. Number WO2006041300 (2006).
[14] A. Hassan, Patent Appl. Publ. Number WO2006063220 (2006).
[15] M. Krumpelt, J.P. Kopasz, S. Ahmed, R.L. Kao, S.S. Randhava, U.S. Patent 6,967,063 (2005).
[16] K.W. Kramarz, I.D. Bloom, R. Kumar, S. Ahmed, R. Wilkenhoener, M. Krumpelt, U.S. Patent 6,303,098 (2001).
[17] P. Erri, P. Dinka, A. Varma, Chem. Eng. Sci. 61 (2006) 5328.
[18] Y. Junhan, C.N. Juan, M.S. Wolfgang, Mater. Lett. 59 (2005) 3645.
[19] M. Shi, N. Liu, Y.D. Xu, C. Wang, Y.P. Yuan, P. Majewski, F. Aldinger, J. Mater. Process. Technol. 169 (2005) 179.
[20] V.V. Zyryanov, V.A. Sadykov, N.F. Uvarov, G.M. Alikina, A.I. Lukashevich, S. Neophytides, J.M. Criado, Solid State Ionics 176 (2005) 2813.
[21] K.C. Patil, S. Aruna, T. Mimani, Curr. Opin. Solid State Mater. Sci. 6 (2002) 507.

[22] K.C. Patil, S. Aruna, S. Ekambaram, Curr. Opin. Solid State Mater. Sci. 2 (1997) 158.
[23] P. Dinka, A. Mukasyan, Proceedings of the NSTI Nanotechnology Conference 1, 2006, p. 456.
[24] A. Mukasyan, P. Epstein, P. Dinka, Proc. Comb. Inst. 31 (2007) 1789.
[25] P. Dinka, A. Mukasyan, J. Phys. Chem. B 109 (2005) 21627.
[26] P. Dinka, A. Mukasyan, Int. J. Self-Propag. High Temp. Synth., in press.
[27] C.J. Montgomery, S.M. Cannon, M.A. Mawid, B. Sekar, 40th AIAA Aerospace Sciences Meeting and Exhibit, Reno, Nevada 0336, 2002.
[28] J. Scheidtmann, P.A. Wei, F. Maier, Appl. Catal. A: Gen. 222 (2001) 79.
[29] J. Sehested, J.A.P. Gelten, I.N. Remediakis, H. Bengaard, J.K. Norskov, J. Catal. 223 (2004) 432.
[30] K. Urasaki, Y. Sekine, S. Kawabe, E. Kikuchi, M. Matsukata, Appl. Catal. A: Gen. 286 (2005) 23.
[31] J. Sehested, Catal. Today 111 (2006) 103.
[32] D.L. Trimm, Catal. Today 37 (1997) 233.
[33] D.L. Trimm, Catal. Today 49 (1999) 3.
[34] L. Wang, K. Murata, M. Inaba, Appl. Catal. A: Gen. 257 (2004) 43.